

Alma Mater Studiorum Università di Bologna  
Archivio istituzionale della ricerca

Open-cell foams coated by Ni/X/Al hydrotalcite-type derived catalysts (X = Ce, La, Y) for CO<sub>2</sub> methanation

This is the final peer-reviewed author's accepted manuscript (postprint) of the following publication:

*Published Version:*

Ho, P.H., Sanghez de Luna, G., Ospitali, F., Fornasari, G., Vaccari, A., Benito, P. (2020). Open-cell foams coated by Ni/X/Al hydrotalcite-type derived catalysts (X = Ce, La, Y) for CO<sub>2</sub> methanation. JOURNAL OF CO<sub>2</sub> UTILIZATION, 42, 1-11 [10.1016/j.jcou.2020.101327].

*Availability:*

This version is available at: <https://hdl.handle.net/11585/778146> since: 2023-05-18

*Published:*

DOI: <http://doi.org/10.1016/j.jcou.2020.101327>

*Terms of use:*

Some rights reserved. The terms and conditions for the reuse of this version of the manuscript are specified in the publishing policy. For all terms of use and more information see the publisher's website.

This item was downloaded from IRIS Università di Bologna (<https://cris.unibo.it/>).  
When citing, please refer to the published version.

(Article begins on next page)

This is the final peer-reviewed accepted manuscript of:

**Open-cell foams coated by Ni/X/Al hydrotalcite-type derived catalysts (X = Ce, La, Y) for CO<sub>2</sub> methanation, P. H. Ho, G. Sanghez de Luna, F. Ospitali, G. Fornasari, A. Vaccari, P. Benito, Journal of CO<sub>2</sub> Utilization, 42 (2020) 101327**

The final published version is available online at:  
<https://doi.org/10.1016/j.jcou.2020.101327>

#### Terms of use:

Some rights reserved. The terms and conditions for the reuse of this version of the manuscript are specified in the publishing policy. For all terms of use and more information see the publisher's website.

*This item was downloaded from IRIS Università di Bologna (<https://cris.unibo.it/>)*

***When citing, please refer to the published version.***

## **Open-cell foams coated by Ni/X/Al hydrotalcite-type derived catalysts (X = Ce, La, Y) for CO<sub>2</sub> methanation**

Phuoc Hoang Ho<sup>§</sup>, Giancosimo Sanghez de Luna, Francesca Ospitali, Giuseppe Fornasari, Angelo Vaccari, Patricia Benito\*

Dipartimento Chimica Industriale “Toso Montanari”, Università di Bologna, Viale Risorgimento 4, 40136, Bologna, Italy

<sup>§</sup>Present address: Chemical Engineering, Competence Center for Catalysis, Chalmers University of Technology, S-412 96, Gothenburg, Sweden.

\* patricia.benito3@unibo.it

## Abstract

NiAl hydrotalcite-type materials containing rare-earth elements (La, Ce, Y) are coated on thermal conductive NiCrAl open-cell foams by the electrodeposition method. After calcination and reduction at 600 °C, the obtained structured materials have a stable coating wherein Ni nanoparticles are well-dispersed. Consequently, the catalysts with rare-earth elements show a remarkable activity enhancement in the CO<sub>2</sub> methanation in comparison to a NiAl catalyst. At 325 °C (oven temperature) CH<sub>4</sub> productivity rates of 6.75 – 8.35 mole g<sub>Ni</sub><sup>-1</sup> h<sup>-1</sup> (38,200 h<sup>-1</sup>, CO<sub>2</sub>/H<sub>2</sub>/N<sub>2</sub> = 1/4/1 v/v) are achieved. Ce has the largest effect on the improvement of the CO<sub>2</sub> conversion and stability (also feeding a N<sub>2</sub> free feedstock) followed by Y and La, due to the balance between the amount and activity of the catalytic coating. The Ce structured catalyst is also more active and selective than its pelletized counterpart at similar outlet temperature. Temperature profiles recorded along the centerline of the catalytic bed provide an overview of hotspot formation that plays an important role in the control of activity/selectivity and catalyst deactivation.

**Keywords:** CO<sub>2</sub> methanation, Ni-based catalysts, open-cell foams, rare-earth element, electrodeposition

## 1. Introduction

The hydrogenation of CO<sub>2</sub> to CH<sub>4</sub> (methanation or Sabatier reaction), using H<sub>2</sub> coming from electrolysis of water powered by renewable energy, produces a gas that can be directly injected into the grid or used as a transport fuel whenever the H<sub>2</sub> content is in the range of 0 – 12 vol.% (< 1 vol.% in Belgium/UK/Sweden, 6 vol.% in France, or 12 vol.% in Holland [1]). The exothermic methanation is favored at low temperature; while above 450 °C the endothermic reaction of CO<sub>2</sub> with H<sub>2</sub> to form CO (reverse water gas shift, RWGS) becomes important, decreasing the CH<sub>4</sub> selectivity [2]. To achieve a high conversion/selective/stable process two obstacles need to be tackled: to find a suitable catalyst [3,4] and to deal with the heat developed (due to the exothermicity of the process) inside the catalytic bed [5-8]. Nickel catalysts are widely investigated for the CO<sub>2</sub> methanation [9]. Among them we can find bulk hydrotalcite-derived (HT) catalysts that are more active [10] and stable than commercial impregnated catalysts [11] since, even at high Ni loadings, are characterized by a high dispersion and stability of Ni<sup>0</sup> particles [12,13]. These properties are improved by adding rare-earth elements, which also provide basic sites for the CO<sub>2</sub> activation [14,15]. On the other hand, keeping the temperature under control during methanation means avoiding hot-spots, damage of the construction materials and catalysts, thermal runaway of the reactor, and, very important, achieving high conversions and selectivities, since the process is thermodynamically favored at low temperature.

Structured catalysts are an appealing option to simultaneously tackle the activity and heat transfer issues. A catalyst made of a 3D support coated by a highly active methanation catalyst layer, besides selectively converting CO<sub>2</sub> to CH<sub>4</sub>, may enhance the heat (and mass) transfer, decrease the pressure drop and allow to work under transient conditions [16]. Hence, structured catalysts could be feasible solution to operate the methanation reaction in a compact and fast response reactor within the Carbon Capture and Utilization chain [17].

The enhancement of the heat management inside the methanation reactor by structured catalysts has been demonstrated in several works (e.g. [18-21]), even in the scale-up of the process [22,23]. Nevertheless, some aspects require further improvement both from the chemical and chemical-engineering point of view. The development of structured catalysts is not straightforward since their activity and stability are the interplay of several factors [16,24]. The performance is related to: i) the chemical nature and morphology of the coating, which also depend on the preparation method; ii) the properties of the support (material, shape, geometry), and iii) the adhesion and interaction between coating and support.

Metallic supports provide higher effective thermal conductivity and better mechanical strength than their ceramic counterparts [16]. In a Ni/CeO<sub>2</sub> structured catalyst for the CO<sub>2</sub> methanation, an Al honeycomb fin support favors the heat transfer and in turn decreases the differences between set and actual temperature in the bed in comparison to pelletized catalysts [25]. The cell density and the configuration of the fin determine the activity [26,27]: in a stacked and preferably in a multistacked-type-fin configuration, the random flow channels enhance mass transfer properties and, under industrial-type conditions only generate a moderate hot spot (lower than the Tamman temperature of nickel particles). NiMgAl HT-derived catalysts coated on an Inconel heat exchanger, wherein opposing corrugated plates distribute the flow homogeneously inside each reaction channel and over the entire reactor, control the reaction temperature and avoid temperature runaway [28]. Moreover, the combination of an Al-honeycomb followed by a stainless-steel honeycomb coated by Ni/Al<sub>2</sub>O<sub>3</sub> takes advantage from the high specific production rate of the Al part and the low radial conductivity of the steel part, which avoid fast cooling of the gas and, hence, a high CO<sub>2</sub> conversion is reached [20].

Open-cell foams, Al (40 ppi) [22,29] or Ni (100 ppi) [30], with a tortuous flow path, also provide a better thermal management, though its effect on the catalytic performance is not always evident. For instance, in a comparison among fixed-bed, millistructured, and metallic foam reactors

with the same NiAl catalyst coating [29], the Al foam shows very good thermal management, due to the high equivalent thermal conductivity of the Al support combined with a low catalyst load, but a much lower space-time yield and volumetric productivity than fixed bed and millistructured reactors. By comparing Ni-CeO<sub>2</sub>-ZrO<sub>2</sub> and NiO-Al<sub>2</sub>O<sub>3</sub> coated on Al [22] and Ni [30] foams, respectively, with their pelletized bed counterparts, a lower temperature increase in the bed is observed for the structured catalysts, while the productivity or activity is similar than for pelletized catalysts. In some cases, the amount of catalyst in the coating may be responsible for the low activity, as reported for NiCrAl foams (450 to 1200  $\mu\text{m}$  cell size, 130 to 45 ppi) coated by a Co-Al<sub>2</sub>O<sub>3</sub> xerogel [31]. Actually, Ricca et al. reported that an Al foam coated by a 5 wt.% Ni/CeO<sub>2</sub>-ZrO<sub>2</sub> catalyst outperforms a pelletized catalyst due to a more effective heat transfer from warmer to colder areas in the bed [32]; however, in comparison to a SiC honeycomb monolith, it shows a lower heat transfer due to the lower effective thermal conductivity of the foam, which is made by large pores (20 ppi Al foam). It is worthy to note that the effective thermal conductivity of metallic open-cell foams could be improved using high-density cell materials [16]. Moreover, high-cell density foams provide a larger geometric surface available for the deposition of the catalytic coating, and in turn can increase the amount of active phase in the structured catalyst.

The aim of this work is to prepare open-cell foam-based catalysts that combine a catalytic coating highly active at low temperature in the CO<sub>2</sub> methanation and an enhanced heat transfer support. Hence, we propose structured catalysts made by HT-derived NiAl coatings modified by rare-earth elements (Ce, La, Y) deposited on commercial NiCrAl open-cell foams with high cell density (450  $\mu\text{m}$  nominal cell size, 130 ppi). The coatings are prepared by electrodeposition (the electro-base generation method [33]) followed by calcination. The effect of rare-earth elements (Ce, La, and Y) on the chemical-physical properties of the coating and their catalytic performance (activity and stability) in CO<sub>2</sub> methanation at high space velocity are firstly studied, relating the results with those previously reported for coprecipitated catalysts [15]. Next, the role of the structured support is

investigated by comparing the most active catalyst with its coprecipitated pelletized bed counterpart, also considering temperature profiles along the centerline of the catalytic bed.

## 2. Experimental section

### 2.1 Structured catalyst preparation

From a commercial panel of NiCrAl foam (1.6 mm thickness and 450  $\mu\text{m}$  cell size from Alantum), disks of 10 mm diameter were cut and a 2 mm hole was made in the center to insert a thermo-well during catalytic tests. The disks were then washed with acetone, distilled water, and afterwards dried at 40 °C for 24 h. Prior to the electrodeposition, the foam surface was activated by chemical treatment in HCl 5 M for 15 min to remove surface oxides, this step is important for improving the electrodeposition [34]. After the treatment, the foams were washed thoroughly with ultra-pure distilled water. The electrodeposition was performed in a double compartment electrochemical flow cell described elsewhere [33], using a potentiostat (Autolab, PGSTAT128N, Eco Chemie) with GPES software. A Pt coil (0.4 mm diameter and 40 cm length) and a saturated calomel electrode (SCE) were used as counter and reference electrodes (C.E. and R.E.), respectively. The working electrode was the NiCrAlloy foam disk and it was assembled by a two-pronged Pt electrical contact.

The electrolytes were aqueous solutions of: i)  $\text{Ni}(\text{NO}_3)_2$  and  $\text{Al}(\text{NO}_3)_3$  with  $\text{Ni}/\text{Al} = 75/25$  atomic ratio (a.r.) to prepare the NiAl HT precursors (NiAl-HT); ii)  $\text{Ni}(\text{NO}_3)_2$ ,  $\text{X}(\text{NO}_3)_3$  and  $\text{Al}(\text{NO}_3)_3$ , where  $\text{X} = \text{La}, \text{Y}, \text{Ce}$ , and with  $\text{Ni}/\text{X}/\text{Al} = 70/5/25$  a.r., to prepare HT compounds modified by rare-earth elements (NiXAl-HT). The total metal concentration of the electrolytes was 0.06 M. The syntheses were performed at -1.3 V vs SCE for 750 s and 2  $\text{mL min}^{-1}$  of electrolyte flow rate. After coating, the foams were rinsed in distilled water followed by drying at 40 °C for 24 h. Eventually, the coated foams were calcined at 600 °C in static air for 6 h and the structured catalysts named as NiAl or NiXAl (where  $\text{X} = \text{La}, \text{Y}, \text{Ce}$ ), respectively.



For comparison purposes, a NiCeAl pellet catalyst with the same nominal composition (Ni/Ce/Al = 70/5/25 a.r.) was also prepared by co-precipitation. Detailed information of preparation and physical-chemical properties of this catalyst can be found in our previous work [15].

## 2.2 Characterization techniques

Scanning electron microscopy (SEM) coupled to energy dispersive spectrometry (EDS) was performed by using an EP EVO 50 Series Instrument (EVO ZEISS) equipped with an INCA X-act Penta FET® Precision EDS microanalysis and INCA Microanalysis Suite Software (Oxford Instruments Analytical) to provide images of the spatial variation of elements in a sample. The accelerating voltage was 20 kV and the spectra were collected in duration 60 s. Due to the overlapped composition of Ni and Al between the coating and the NiCrAl support, the coating powder was removed from the foam and it was subsequently analyzed by EDS.

Porosity of the structured catalysts was determined by N<sub>2</sub> adsorption/desorption at -196 °C using a Micromeritics ASAP 2020 instrument. Samples (two calcined coated foams) were degassed under vacuum (< 30 µm Hg) up to 250 °C and maintained for 30 min before performing the measurement. The specific surface area (S<sub>BET</sub>) was calculated using the Brunauer-Emmett-Teller (BET) multiple-point method in the relative pressure range  $p/p^0$  from 0.05 to 0.3.

Hydrogen temperature programmed reduction (H<sub>2</sub>-TPR) was performed in an AutoChem II (Chemisorption analyzer, Micromeritics). The structured catalyst (two calcined coated foams containing ca. 10-15 mg of coating) was firstly pretreated at 150 °C under 30 mL min<sup>-1</sup> of He for 30 min. After cooling to 40 °C under He, the carrier gas was switched to 5 % H<sub>2</sub>/Ar (v/v) at 30 mL min<sup>-1</sup>. When the baseline was stable, the temperature was increased to 900 °C with a ramp of 10 °C min<sup>-1</sup>. The effluent gas passed through an ice-cold trap, afterwards the H<sub>2</sub> consumption was measured by means of a thermal conductivity detector (TCD).

High resolution transmission electron microscopy (HRTEM) characterization was carried out by a TEM/STEM FEI TECNAI F20 microscope, equipped with an EDS analyzer. The solid coating scratched from the foam catalysts was suspended in ethanol under ultrasounds for 20 min. The suspension was subsequently deposited on a Cu grid with lacey quanti-foil carbon film and dried at 100 °C before doing the measurement. Selected area electron diffraction (SAED) and Fast Fourier transformation (FFT) were applied to determine the interplanar spacing of the crystals. Particle size distribution was processed considering around 150 particles in three different zones for each sample; EDS analysis was performed to confirm that the particles were made by Ni.

### **2.3 Catalytic tests of CO<sub>2</sub> methanation**

The CO<sub>2</sub> methanation tests were performed in a quartz reactor (ID 10.0 mm) with three foam catalysts, resulting in a 4.8 mm catalytic bed. To measure the temperature profile, a 2 mm thermowell (quartz tube) was inserted into the middle of the catalytic bed. A thermocouple (K-type) can manually slide inside the thermowell allowing to measure the temperature along the length of the catalytic bed during the tests. The catalyst was reduced in 200 mL min<sup>-1</sup> of H<sub>2</sub>/N<sub>2</sub> = 1/1 (v/v) at 600 °C for 2 h. After cooling down to 250 °C and stabilizing at this temperature for 30 min, the feed gas (CO<sub>2</sub>/H<sub>2</sub>/N<sub>2</sub> = 1/4/1 or 1/4/0 v/v) with a total flow rate of 240 mL min<sup>-1</sup> was fed to the reactor. This condition generated a gas hourly space velocity (GHSV) of 38,200 h<sup>-1</sup> (GHSV = total flow rate / apparent volume of the foam bed). For NiAl catalyst, the effect of GHSV was also studied on 6 coated foams by increasing the total flow rate from 240 to 360, or 480 mL min<sup>-1</sup>, which corresponded to 19,100, 28,500 or 38,200 h<sup>-1</sup> of GHSV, respectively. The reaction was carried out from 250 to 425 °C oven temperature with an interval of 25 °C. After passing through a cold trap for water condensation, the outlet stream was analyzed on-line by a PerkinElmer Autosystem XL gas chromatograph, equipped with two thermal conductivity detectors (TCD) and two Carbo-sphere columns using He as a carrier gas for CO, CH<sub>4</sub> and CO<sub>2</sub> quantification, and N<sub>2</sub> for H<sub>2</sub> analysis. Since no C<sub>2</sub>+ hydrocarbons were detected, CO<sub>2</sub> conversion, CH<sub>4</sub> and CO selectivity were defined as follows [35]:

$$\text{CO}_2 \text{ conversion (\%)} = \frac{[\text{CH}_4] + [\text{CO}]}{[\text{CH}_4] + [\text{CO}] + [\text{CO}_2]} \times 100$$

$$\text{CO selectivity (\%)} = \frac{[\text{CO}]}{[\text{CH}_4] + [\text{CO}]} \times 100$$

$$\text{CH}_4 \text{ selectivity (\%)} = \frac{[\text{CH}_4]}{[\text{CH}_4] + [\text{CO}]} \times 100$$

In which [A] (A = CH<sub>4</sub>, CO, CO<sub>2</sub>) represents for molar ratio of component A in the outlet stream.

One blank test is performed with three uncoated calcined foams and no CO<sub>2</sub> conversion is observed, evidencing that the supports are inactive and hence the activities of the structured catalysts are only due to the coating layers.

For the stability test, the catalyst was tested under different reaction conditions with 8 cycles of start-up and shut-down the reactor. After testing in a diluted gas mixture (CO<sub>2</sub>/H<sub>2</sub>/N<sub>2</sub> = 1/4/1 v/v) at different temperatures from 250 to 425 °C, the reaction was shut down and the catalyst was kept under 100 mL min<sup>-1</sup> of N<sub>2</sub>. In the next three days, the reaction was carried out at 325 °C of oven temperature feeding the diluted gas mixture for 9 h each day. The procedure was repeated in the same way, but the reaction was performed in a concentrated gas mixture (CO<sub>2</sub>/H<sub>2</sub>/N<sub>2</sub> = 1/4/0 v/v).

For comparison purposes, some tests were also performed on a NiCeAl pellet catalyst prepared by co-precipitation (specific surface area 159 m<sup>2</sup> g<sup>-1</sup>). After calcination, the catalyst powder was pressed and sieved to collect a particle size in the range of 0.420-0.595 mm. The tests over the pelletized catalyst were performed keeping both the volume of the bed and the amount of catalyst constant in comparison to those over structured catalysts. Hence, 21 mg of pelletized catalyst (similar to the amount of coating on 3 foams) was diluted with 470 mg of quartz (with the same particle size of the pellet) to have a 4.8 mm height bed.

### 3. Results and discussion

#### 3.1. Characterization of coated samples

The electrodeposition at -1.3 V vs SCE for 750 s leads to the generation of a basic media in the vicinity of the foam [36] and in turn the precipitation and deposition of 6-10  $\mu\text{m}$  layers of hydrotalcite-type nanoparticles on the foam surface occur [37], as depicted in Fig. S1. This behavior is independent on the type of rare-earth element. The solid compositions are close to those in the electrolytic solutions for all the materials, excluding the La-containing sample that is richer in Al than in Ni (Table 1). The cracks in the coatings are related to both the drying process and  $\text{H}_2$  bubbles that evolve due to the electrochemical reduction of water, the latter occurs as a side-reaction during the electrodeposition [36]. Solid loadings slightly depend on the rare-earth element, i.e. 10 – 11 wt.% for NiAl and NiLaAl, but 12.3 and 13.6 wt.% for NiYAl and NiCeAl, respectively (Table 1). Note that the aim of this work is not to keep constant the amount of electrodeposited material, but the deposition conditions.

The catalytic coatings, obtained after calcination at 600 °C for 6 h, are made of nanoparticles of poor crystallized NiO or NiAlO<sub>x</sub> phases (Fig. 1 and Fig. S2), which are characteristic of HT-derived catalysts. The low intensity and broadness of the reflections made it not possible to obtain any information about the effect of  $\text{Ce}^{4+}$ ,  $\text{Y}^{3+}$  and  $\text{La}^{3+}$  on the catalyst structure. However, in agreement with our previous work [15], dealing with the same coprecipitated catalysts, it is expected that well dispersed patches of  $\text{La}_2\text{O}_3$  and  $\text{CeO}_2$  are present in La and Ce-containing materials, while  $\text{Y}^{3+}$  could be located inside the oxidic matrix. The coatings are mesoporous solids with Type IV  $\text{N}_2$  adsorption/desorption isotherms (Fig. S3) and their estimated specific surface areas are around 119-150  $\text{m}^2 \text{g}^{-1}_{\text{coating}}$  (Table 1). On the other hand, the foam support contains NiCr,  $\text{Ni}_{0.9}\text{Al}_{1.1}$ , and  $\text{Ni}_3\text{Al}$  crystalline phases (Fig. S2), the two latter are strengthening agents that improve the oxidation resistance at high temperature of the support [38]. During calcination, the weight loss of ca. 4 – 6 wt.%, occurring due to the decomposition of the hydroxides (Table 1), and the shearing stresses provoke a partial solid detachment.

Ni species are reduced in the 350-800 °C temperature range during H<sub>2</sub>-TPR experiments (Fig. 2), characteristic of Ni species well stabilized inside the oxide matrix [39]. The small peak at low temperature could be related to the removal of residual carbonates or water or to the reduction of some Ni<sup>3+</sup> species present in a non-stoichiometric NiO [40]. The NiCrAl foam does not contribute to the H<sub>2</sub> consumption since a flat profile is recorded for the bare calcined foam. The broad H<sub>2</sub> consumption signal suggests the presence of overlapped Ni reduction steps, which are slightly modified depending on the rare-earth element. Nevertheless, it is challenging to correlate the differences in the reduction profiles to the interaction of Ni species with the oxide matrix, since the above commented differences in chemical composition, amount of coating and surface area, may also modify the reduction profiles. Moreover, the 600 °C calcination temperature is overcome during the experiments, hence, the interaction between the catalytic coating and the support, e.g. the formation of NiAl<sub>2</sub>O<sub>4</sub>, could not be excluded [41]. Note that in our previous work dealing with coprecipitated HT-derived catalysts, rare-earth elements do not have any remarkable effect on the reducibility of Ni<sup>2+</sup> [15]. Furthermore, for coprecipitated catalysts, the reduction occurs at higher temperatures (ca. 50 - 100 °C) than in the present work, probably due to the higher amount of catalyst used during the experiments with pelletized catalysts rather than to modifications in the reducibility of Ni species.

### 3.2 Catalytic tests

Rare earth elements increase the activity and selectivity throughout all the oven temperature range investigated (Fig. 3), the differences being more remarkable below T<sub>oven</sub> = 325 °C, which can be considered the kinetic-limited region. The Ce-containing catalyst is the most active, it achieves a 41 % CO<sub>2</sub> conversion already at 250 °C oven temperature in comparison to only 5 % for Y- and La-modified catalysts (Fig. 3a). The promotion effect of Y and La becomes important at 275 °C, though it is always lower than for Ce. The expected decrease in the conversion by increasing the oven temperature (e.g. higher than 325 °C) is more remarkable for Ce, La and Y catalysts, suggesting that they reached earlier the thermodynamic equilibrium. Selectivity in CH<sub>4</sub> also depends on the type of

catalyst as depicted in Fig. 3b. The more active is the catalyst, the more selective is the CH<sub>4</sub> formation, though the effect of the catalyst composition on the selectivity is not as remarkable as on the conversion. The contribution of the RWGS becomes more important above 325 °C, CO production increases by ca. 1.0-1.5 %; however, CH<sub>4</sub> selectivity values for all the promoted catalysts are still above 95 % at temperatures below 400 °C.

The catalytic coating loadings slightly depend on the type of rare-earth element, and consequently the space velocity values (referred to the amount of catalyst) are modified. This feature could partially explain the different activity trend observed for structured catalysts in comparison to coprecipitated pelletized catalysts, i.e. Ce > Y $\approx$ La > NiAl for foams and La > Ce > Y > NiAl for pellets [15]. The CH<sub>4</sub> productivity rate at T<sub>oven</sub> = 250 °C is higher for the NiCeAl catalyst (NiCeAl: 3.50; NiLaAl: 0.64; NiYAl: 0.69; and NiAl: 0.22 mol CH<sub>4</sub> g<sub>Ni</sub><sup>-1</sup> h<sup>-1</sup>). Conversely, at T<sub>oven</sub> = 325 °C, namely under conditions close to a real application (though the thermodynamic equilibrium has not been reached), the NiLaAl outperforms the NiCeAl in term of productivity (Table 2) probably due to its lower catalytic coating loading and/or some thermal effects. However, it is worth to note that, as shown in Table 2, all the catalysts here prepared reach outstanding CH<sub>4</sub> production rates (6.75 – 8.35 mol g<sub>Ni</sub><sup>-1</sup> h<sup>-1</sup>) in comparison to the results reported in the literature operating at 1 and 5 bar.

The productivities could be related to the interplay among a highly active catalytic coating and a small pore size foam, but also to the reaction conditions. Open-cell foams show an enhanced mass and heat transfer in comparison to honeycomb monoliths; moreover, the smaller the pore size, the higher the efficient thermal conductivity of the metallic foams [42]. Note that the foam supports in the literature used for the CO<sub>2</sub> methanation are usually ceramic and with a large pore size (e.g. 40 ppi in ref 45). The large geometric surface area of the metallic foams (related to the small pore size) and the use of HT derived catalysts allowed us to prepare active structured catalysts even with a thin coating layer (i.e. 6-10 μm vs 5-20 μm in ref 33 and 20-35 μm in ref 45), which enhances mass transfer. The structured catalysts containing a high Ni loading, but well dispersed and stabilized Ni

nanoparticles (see characterization of spent catalyst), are highly active and selective to CH<sub>4</sub> at low oven temperatures, which increase the productivity rate. However, the CH<sub>4</sub> production rates also depend on the reaction conditions, namely high space velocities and concentrated feedstocks increase the productivity [27,43, 45]; moreover, the effect of the heat developed could not be discarded. In the present work, we are using high space velocity values in comparison to most of the works reported in Table 2; the only exceptions are the tests on Ni/CeO<sub>2</sub> honeycomb fin at GHSV = 11,459 and 8021 h<sup>-1</sup> (600 and 420 L g<sub>coating</sub><sup>-1</sup> h<sup>-1</sup> referred to the amount of coating) that also reach high productivity rates (30.51 and 20.23 mole<sub>CH<sub>4</sub></sub> g<sub>Ni</sub><sup>-1</sup> h<sup>-1</sup>) [27]. These reaction conditions and the high activity of the catalysts provoke an increase in the temperature in the catalytic bed (*vide infra*), which could foster the reaction in the low temperature kinetic-limited region [27]. However, it is worth to note that if the temperature increases to a certain high value at which the exothermic reaction is unfavored, the CO<sub>2</sub> conversion decreases.

The role of the space velocity on the performance was investigated over the least active NiAl structured catalyst by modifying the total flow rate. In Fig. 14 it is shown that CO<sub>2</sub> conversion is largely affected by the space velocity at T<sub>oven</sub> = 300 °C, e.g. it is 13 and 64 % at 38,200 and 19,100 h<sup>-1</sup>, respectively; moreover, a 99 % selectivity in CH<sub>4</sub> is reached at 19,100 h<sup>-1</sup>. Above 300 °C, the contribution of the temperature inside the catalytic bed may smooth the differences among catalysts, but the same trend is observed in the conversion values. These results suggest that selecting both the optimum flow rate and coating loading, the activity could be further increased.

The heat developed by the exothermic reaction provokes an increase in the temperature in the catalytic bed. The temperature profiles measured at the centerline of the bed for all the catalysts are displayed in Fig. 5a and Fig. S4. As expected, the temperature increment, calculated as T<sub>max</sub>-T<sub>oven</sub>, is related to the CO<sub>2</sub> conversion (Fig. 5b). While the position of the maximum temperature reached depends on the catalyst composition (Fig. S4). For instance, for NiLaAl, whatever the set oven temperature is, the maximum temperature is registered at 2 mm from the inlet, while for NiCeAl

sample it is at the outlet of the bed. The different amounts of heat developed for all the catalysts may mask the real catalyst activity and productivity trend, mainly in the kinetic limited regions, since the temperature besides a consequence can be a cause of the reaction [27,44]. However, when plotting the conversion of CO<sub>2</sub> versus the outlet temperature, the trend is similar to that obtained by plotting the CO<sub>2</sub> conversion versus the oven temperature, mainly at low oven temperature (Fig. S5).

In the literature, both steep and flat temperature profiles are measured for structured catalysts; however, making an accurate comparison with the works previously reported is tricky. The space velocity, concentration of the reaction gas mixture, activity of the catalyst, as well as the shape and material of the support in the structured catalyst modify the temperature profile, and some of them are different in the works compared. For instance, the flat profile measured for a 50 wt.% Ni/GDC cordierite honeycomb may be related to a low catalyst activity, 42 % conversion of CO<sub>2</sub> at  $T_{\text{oven}} = 300\text{ }^{\circ}\text{C}$  and  $\text{GHSV} = 10,000\text{ h}^{-1}$  [44]. The temperature profile measured along the foam bed in our work for the NiCeAl catalyst is similar to the first 5 cm length of the profile reported by Ratchahat et al. for a multistacked type-fin configuration [27]; note that the latter reaches a high conversion and selectivity, 90 and 99.9 %, respectively, and operates at a lower space velocity. Namely, by setting an oven temperature of  $300\text{ }^{\circ}\text{C}$ , a moderate hotspot of  $130\text{ }^{\circ}\text{C}$  ( $T_{\text{max}} - T_{\text{oven}}$ ) was measured at position 4 mm of the foam bed in this work ( $682\text{ L g}^{-1}\text{ h}^{-1}$ ), while it was  $136\text{ }^{\circ}\text{C}$  at position of 2.5 mm of the honeycomb monolith ( $420\text{ L g}^{-1}\text{ h}^{-1}$ ). A similar hotspot recorded over both foam and honeycomb monolith beds may be related to a balance between conversion and space velocity in the heat development. However, it could also suggest a fast dissipation of heat on the foam bed, although the differences in the scales of the reactor in both studies may also modify the heat transfer. In a recent work, a rather flat temperature profile for an alumina open-cell foam coated with Ni/GDC, not observed over a cordierite honeycomb monolith, is related to a homogeneous distribution of the heat generated by the reaction [45].



The stability of rare-earth containing structured catalysts is investigated within an 8-day test by feeding both diluted ( $\text{H}_2/\text{CO}_2/\text{N}_2 = 1/4/1$  v/v) and concentrated ( $\text{H}_2/\text{CO}_2/\text{N}_2 = 1/4/0$  v/v) feedstock (Fig. 6). The most active Ce-sample is also the most stable, constant 77 %  $\text{CO}_2$  conversion and 98 %  $\text{CH}_4$  selectivity values as well as very stable temperature profiles (Fig. 7a) are recorded during 66 h of time-on-stream (TOS). Note that the temperatures inside the bed (Fig. S4 and Fig. S6), higher in the  $\text{H}_2/\text{CO}_2/\text{N}_2 = 1/4/0$  v/v mixture, can be considered representative to those reached in a reactor operating under real conditions [43]. The similarities in the activity regardless of the concentration of the feedstock can be explained considering that feeding a concentrated gas mixture may have two counter effects on the activity: a higher reactants partial pressure would increase the conversion, while the larger amount of heat generated would decrease it (at oven temperature above 300 °C). Remarkably, the stability of the NiCeAl structured catalyst with TOS is similar to that reached with a more expensive 10 wt.% Ru/ $\text{Al}_2\text{O}_3$ /honeycomb monolith with 8 shut-down/start-up cycles (72 h of TOS) in a more diluted gas mixture ( $\text{CO}_2/\text{H}_2/\text{He} = 4/16/80$  v/v, GHSV = 4720  $\text{h}^{-1}$ , 217 °C, 1 bar) [46]. Contrarily, Y- and La-containing samples slightly deactivate in the concentrated feed, as evidenced by a 1.3 – 1.7 % decrease in the conversion and a steadily production of CO (selectivity moves from 2.9 to 3.2 and 3.3 to 3.6 % for La and Y, respectively). Consequently, the temperature slightly decreases with TOS (Fig. 7b and 7c), either because of decrease in the  $\text{CO}_2$  conversion to  $\text{CH}_4$  or to a higher contribution of the endothermic RWGS.

### 3.3. Structured vs pelletized catalysts

To better investigate the advantages of structured catalysts in the  $\text{CO}_2$  methanation, the Ce-containing catalyst is compared with its pelletized counterpart prepared by coprecipitation. The tests are performed keeping constant the catalytic bed volume and catalyst amount as well as the total flow rate. The structured catalyst outperforms the pelletized one, throughout all the temperature range investigated, in term of both conversion and selectivity as shown in Fig. 8. For instance, at  $T_{\text{oven}} = 275$  °C  $\text{CO}_2$  conversion and  $\text{CH}_4$  selectivity are around 27.0 and 3.6 % higher for the structured

catalyst, respectively, accordingly, the CH<sub>4</sub> productivity increases in around 56.0 %. Notably, the structured catalyst bed also outperforms a pelletized bed containing an amount of catalyst larger than that in the foam coating (Fig. 8a, 8b).

The type of catalyst (structured or pellet), as depicted in Fig. 9, modifies both the temperature along the bed (due to differences in activity) and the shape of the profile (a plateau at the end of the bed for the structured catalyst while a steadily temperature increase for pellets). The temperature gradient of 15 °C in the case of the pelletized catalyst is comparable with results recently reported by Italiano et al. [47], but under milder reaction conditions than in the present work (about one-fourth of GHSV and more diluted of feedstock, CO<sub>x</sub>/H<sub>2</sub>/N<sub>2</sub> = 1/4/5 v/v).

Interestingly, the plot of the CO<sub>2</sub> conversion versus the outlet temperature in Fig. S7, reveals that at a similar outlet temperature, conversion is higher over foams than pellets, and only reach the formers the thermodynamic equilibrium. These results suggest that the temperature increase is not responsible of the trend observed in the activity, it could be related to an increase in heat transfer in the structured reactor. However, the effect of an enhanced mass transfer and coating properties could not be neglected.

### 3.4. Characterization of spent catalysts

Catalytic coatings are not largely modified during tests, as shown in SEM images displayed in Fig. S8, catalyst homogeneity and particle size are rather similar than for fresh samples reported in Fig. 1. Note that NiLaAl, NiYAl, and NiCeAl are spent after longer TOS values than NiAl due to the stability tests performed.

Despite Ni catalysts derived from HT-type compounds have a low tendency to form carbonaceous deposits [15,48], in some locations of the NiAl foam placed at the inlet of the bed, Raman spectra display bands at around 1335 and 1610 cm<sup>-1</sup> due to carbonaceous species (Fig. S9).

HRTEM images of the coating scratched from the foams show ill-defined Ni nanoparticles in all the investigated samples (Fig. 10). SAED analysis confirms the presence of Ni<sup>0</sup> in the spent catalyst, which coexists with NiO (Fig. S10), the latter could be related to the oxidation of the catalyst during handling [15]. The rare-earth elements clearly decrease the Ni particle size (insets Fig. 10). The NiAl catalyst contains a broad distribution of particles around 7.8 nm ± 3.1 nm, note that this catalyst was tested for 8 h instead of 66 h for rare-earth containing samples. Remarkably, these particles are larger than those present in its NiAl spent coprecipitated counterpart (4.9 nm ± 2.8 nm) [15], which may explain the formation of carbon for the NiAl structured catalyst. The NiYAl catalyst shows the smallest particle size (3.6 ± 2.3 nm), while rather similar average sizes are obtained for NiCeAl (4.4 ± 1.3 nm) and NiLaAl (4.3 ± 1.8 nm) catalysts.

Hence, it could be stated that the advantages of HT-derived catalysts in keeping small and stable Ni particles even at high Ni loadings are also achieved with electrodeposited materials. Rare-earth elements modify the Ni particle size, though the trend obtained is different than for coprecipitated catalysts. For instance, NiAl and NiLaAl structured catalysts show slightly larger particles than the corresponding pelletized catalysts [15]. Hence, the discrepancies observed in the effect of the type of rare-earth element on the activity of pelletized and structured catalysts may be related to the Ni particle size, amount of catalytic coating on structured catalyst (similar catalyst is always used in tests with pellets), and to the temperatures reached in the catalytic bed.

The Ce structured catalyst reaches a higher CO<sub>2</sub> conversion, CH<sub>4</sub> selectivity and productivity in the low temperature range due to the slightly greater loading of a highly active catalytic coating (Table 1). The activity of the coatings is a combination of both Ni particle size and basicity of the support. For the Ce catalyst, the Ce<sup>4+</sup>/Ce<sup>3+</sup> couple also can participate in the CO<sub>2</sub> activation [49]. Unfortunately, CO<sub>2</sub>-Temperature Programmed measurements over structured catalysts did not give any reliable information.

#### 4. Conclusions

Ni bulk catalysts promoted by rare-earth elements are easily deposited on NiCrAl open-cell foams by in situ synthesis of NiAl hydrotalcite-type compounds modified by La, Y, and Ce through electrodeposition followed by calcination. Like in conventional coprecipitated powder catalysts, rare-earth elements do not largely modify the structure, morphology, and reducibility of the NiAl catalyst. However, they help to keep smaller Ni particle sizes after reaction for 66 h (feeding both diluted and concentrated feed gas at GHSV = 38,200 h<sup>-1</sup> and T<sub>oven</sub> = 325 °C) and probably improve the basicity of the catalysts, enhancing, therefore, the performance and stability in the CO<sub>2</sub> methanation. The CH<sub>4</sub> productivity rates achieved on structured catalysts (6.49 – 8.35 mol g<sub>Ni</sub><sup>-1</sup> h<sup>-1</sup>) are promising, in comparison with the results reported in recent literature, due the interplay among a highly active coating, a small pore size foam, and reaction conditions. The Ce-containing catalyst achieves the highest CO<sub>2</sub> conversion and CH<sub>4</sub> selectivity in the low temperature range due to a greater loading of a highly active catalytic coating. The structuration of the catalysts on foams increases the performance in comparison to their pelletized counterpart at similar temperature at the outlet of the catalytic bed, which could be related to an enhanced heat transfer.

## Acknowledgements

We acknowledge Alantum for supplying NiCrAl foams.

## References

- [1] J. Newton, Power-to-Gas and Methanation e pathways to a 'Hydrogen Economy', in: 14TH ANNUAL APGTF WORKSHOP London, 2014. URL, <http://www.apgtf-uk.com/files/workshops/14thWorkshop2014/212JohnNewton.pdf>.
- [2] J. Gao, Y. Wang, Y. Ping, D. Hu, G. Xu, F. Gu, F. Su, A thermodynamic analysis of methanation reactions of carbon oxides for the production of synthetic natural gas, RSC Adv. 2 (2012) 2358–2368. <https://doi.org/10.1039/C2RA00632D>.

- [3] S. Kattel, P. Liu, J. G. Chen, Tuning selectivity of CO<sub>2</sub> hydrogenation reactions at the Metal/Oxide interface, *J. Am. Chem. Soc.* 139 (2017) 9739–9754. <https://doi.org/10.1021/jacs.7b05362>.
- [4] C. Vogt, M. Monai, G. Jan Kramer, Bert M. Weckhuysen, The renaissance of the Sabatier reaction and its applications on Earth and in space, *Nat. Catal.* 2 (2019) 188–197. <https://doi.org/10.1038/s41929-019-0244-4>.
- [5] W. Wei, G. Jinlong, Methanation of carbon dioxide: an overview, *Front. Chem. Sci. Eng.* 5 (2011) 2–10. <https://doi.org/10.1007/s11705-010-0528-3>.
- [6] K. P. Brooks, J. Hu, H. Zhu, Robert J. Kee, Methanation of carbon dioxide by hydrogen reduction using the Sabatier process in microchannel reactors, *Chem. Eng. Sci.* 62 (2007) 1161–1170. <https://doi.org/10.1016/j.ces.2006.11.020>.
- [7] M. Götz, J. Lefebvre, F. Mörs, A. McDaniel Koch, F. Graf, S. Bajohr, R. Reimert, T. Kolb, Renewable Power-to-Gas: A technological and economic review, *Renew. Energy* 85 (2016) 1371–1390. <https://doi.org/10.1016/j.renene.2015.07.066>.
- [8] D. Sun, D. S. A. Simakov, Thermal management of a Sabatier reactor for CO<sub>2</sub> conversion into CH<sub>4</sub>: Simulation-based analysis, *J. CO<sub>2</sub> Util.* 21 (2017) 368–382. <https://doi.org/10.1016/j.jcou.2017.07.015>.
- [9] C. Lv, L. Xu, M. Chen, Y. Cui, X. Wen, Y. Li, C.-e Wu, B. Yang, Z. Miao, X. Hu, Q. Shou, Recent progresses in constructing the highly efficient Ni based catalysts with advanced low-temperature activity toward CO<sub>2</sub> methanation, *Front. Chem.* 8 (2020) article 269. <https://doi.org/10.3389/fchem.2020.00269>.
- [10] S. Abate, C. Mebrahtu, E. Giglio, F. Deorsola, S. Bensaid, S. Perathoner, R. Pirone, G. Centi, Catalytic performance of  $\gamma$ -Al<sub>2</sub>O<sub>3</sub>–ZrO<sub>2</sub>–TiO<sub>2</sub>–CeO<sub>2</sub> composite oxide supported Ni-based catalysts for CO<sub>2</sub> methanation, *Ind. Eng. Chem. Res.* 55 (2016) 4451–4460, <https://doi.org/10.1021/acs.iecr.6b00134>.

- [11] S. Ewald, M. Kolbeck, T. Kratky, M. Wolf, O. Hinrichsen, On the deactivation of Ni-Al catalysts in CO<sub>2</sub> methanation, *Appl. Catal. A Gen.* 570 (2019) 376–386, <https://doi.org/10.1016/j.apcata.2018.10.033>.
- [12] S. Rahmani, M. Rezaei, F. Meshkani, Preparation of highly active nickel catalysts supported on mesoporous nanocrystalline  $\gamma$ -Al<sub>2</sub>O<sub>3</sub> for CO<sub>2</sub> methanation, *J. Ind. Eng. Chem.* 20 (2014) 1346–1352, <https://doi.org/10.1016/j.jiec.2013.07.017>.
- [13] C. Mebrahtu, S. Abate, S. Chen, A.F. Sierra Salazar, S. Perathoner, F. Krebs, R. Palkovits, G. Centi, Enhanced catalytic activity of iron-promoted nickel on  $\gamma$ -Al<sub>2</sub>O<sub>3</sub> nanosheets for carbon dioxide methanation, *Energy Technol.* 6 (2018) 1196–1207, <https://doi.org/10.1002/ente.201700835>.
- [14] D. Wierzbicki, R. Baran, R. Dębek, M. Motak, M.E. Gálvez, T. Grzybek, P. Da Costa, P. Glatzel, Examination of the influence of La promotion on Ni state in hydrotalcite-derived catalysts under CO<sub>2</sub> methanation reaction conditions: Operando X-ray absorption and emission spectroscopy investigation, *Appl. Catal. B Environ.* 232 (2018) 409–419, <https://doi.org/10.1016/j.apcatb.2018.03.089>.
- [15] P. H. Ho, G. Sanghez de Luna, S. Angelucci, A. Canciani, W. Jones, D. Decarolis, F. Ospitali, E. Rodriguez Aguado, E. Rodríguez-Castellón, G. Fornasari, A. Vaccari, A. M. Beale, P. Benito, Understanding structure-activity relationships in highly active La promoted Ni catalysts for CO<sub>2</sub> methanation, *Appl. Catal. B Environ.* 278 (2020) 119256, <https://doi.org/10.1016/j.apcatb.2020.119256>.
- [16] E. Tronconi, G. Groppi, C. G. Visconti, Structured catalysts for non-adiabatic applications, *Curr. Opin. Chem. Eng.* 5 (2014) 55–67, <https://doi.org/10.1016/j.coche.2014.04.003>.
- [17] T. Chwoła, T. Spietza, L. Więclaw-Solny, A. Tatarczuk, A. Krótki, S. Dobras, A. Wilk, J. Tchórz, M. Stec, J. Zdeb, Pilot plant initial results for the methanation process using CO<sub>2</sub> from amine

scrubbing at the Łaziska power plant in Poland, *Fuel* 263 (2020) 116804. <https://doi.org/10.1016/j.fuel.2019.116804>.

[18] J. A. Hernandez Lalinde, J. Jiang, G. Jai, J. Kopyscinski, Preparation and characterization of Ni/Al<sub>2</sub>O<sub>3</sub> catalyst coatings on FeCrAl-loy plates used in a catalytic channel reactor with in-situ spatial profiling to study CO<sub>2</sub> methanation, *Chem. Eng. J.* 357 (2019) 435–446. <https://doi.org/10.1016/j.cej.2018.09.161>.

[19] M. Frey, T. Romero, A.-C. Roger, D. Edouard, Open cell foam catalysts for CO<sub>2</sub> methanation: Presentation of coating procedures and in situ exothermicity reaction study by infrared thermography, *Catal. Today* 273 (2016) 83–90. <https://doi.org/10.1016/j.cattod.2016.03.016>.

[20] S. Danaci, L. Protasova, J. Lefevre, L. Bedel, R. Guilet, P. Marty, Efficient CO<sub>2</sub> methanation over Ni/Al<sub>2</sub>O<sub>3</sub> coated structured catalysts, *Catal. Today* 273 (2016) 234–243. <https://doi.org/10.1016/j.cattod.2016.04.019>.

[21] S. Neuberg, H. Pennemann, V. Shanmugam, R. Thiermann, R. Zapf, W. Gac, M. Greluk, W. Zawadzki, G. Kolb, CO<sub>2</sub> methanation in microstructured reactors – catalyst development and process design, *Chem. Eng. Technol.* 42 (2019) 2076–2084. <https://doi.org/10.1002/ceat.201900132>.

[22] M. Frey, A. Bengaouer, G. Geffraye, D. Edouard, A.-C. Roger, Aluminum open cell foams as efficient supports for carbon dioxide methanation catalysts: pilot-scale reaction results, *Energy Technol.* 5 (2017) 2078–2085. <https://doi.org/10.1002/ente.201700188>.

[23] D. Schollenberger, S. Bajohr, M. Gruber, R. Reimert, T. Kolb, Scale-up of innovative honeycomb reactors for power-to-gas applications – The project Store&Go, *Chem. Ing. Tech.* 90 (2018) 696–702. <https://doi.org/10.1002/cite.201700139>.

[24] G. Pauletto, A. Vaccari, G. Groppi, L. Bricaud, P. Benito, D. C. Boffito, J. A. Lercher, Gregory S. Patience, FeCrAl as a catalyst support, *Chem. Rev.* 2020, <https://doi.org/10.1021/acs.chemrev.0c00149>.

- [25] C. Fukuhara, A. Igarashi, Characterization of performances of the wall-type reactor with plate-fin type nickel catalyst prepared by electroless plating for methanol decomposition, *J. Chem. Eng. Japan* 37 (2004) 415–421. <https://doi.org/10.1252/jcej.37.415>.
- [26] C. Fukuhara, K. Hayakawa, Y. Suzuki, W. Kawasaki, R. Watanabe, A novel nickel-based structured catalyst for CO<sub>2</sub> methanation: A honeycomb-type Ni/CeO<sub>2</sub> catalyst to transform greenhouse gas into useful resources, *Appl. Catal. A Gen.* 532 (2017) 12–18. <https://doi.org/10.1016/j.apcata.2016.11.036>.
- [27] S. Ratchahat, M. Sudoh, Y. Suzuki, W. Kawasaki, R. Watanabe, C. Fukuhara, Development of a powerful CO<sub>2</sub> methanation process using a structured Ni/CeO<sub>2</sub> catalyst, *J. CO<sub>2</sub> Util.* 24 (2018) 210–219. <https://doi.org/10.1016/j.jcou.2018.01.004>.
- [28] F. Vidal Vázquez, J. Kihlman, A. Mylvaganam, P. Simell, M.-L. Koskinen-Soivi, V. Alopaeus, Modeling of nickel-based hydrotalcite catalyst coated on heat exchanger reactors for CO<sub>2</sub> methanation, *Chem. Eng. J.* 349 (2018) 694–707. <https://doi.org/10.1016/j.cej.2018.05.119>.
- [29] A. Bengaouer, J. Ducamp, I. Champon, R. Try, Performance Evaluation of fixed-bed, millistructured, and metallic foam reactor channels for CO<sub>2</sub> methanation, *Can. J. Chem. Eng.* 9 (2018) 1937–1945. <https://doi.org/10.1002/cjce.23140>.
- [30] Y. Li, Q. Zhang, R. Chai, G. Zhao, Y. Liu, Y. Lu, F. Cao, Ni-Al<sub>2</sub>O<sub>3</sub>/Ni-foam catalyst with enhanced heat transfer for hydrogenation of CO<sub>2</sub> to methane, *AIChE J.* 61 (2015) 4323–4331. <https://doi.org/10.1002/aic.14935>.
- [31] M. Schubert, L. Schubert, A. Thomé, L. Kiewidt, C. Rosebrock, J. Thöming, F. Roessner, M. Bäumer, Coatings of active and heat-resistant cobalt-aluminium xerogel catalysts, *J. Colloid Interf. Sci.* 477 (2016) 64–73. <https://doi.org/10.1016/j.jcis.2016.05.006>.



- [32] A. Ricca, L. Truda, V. Palma, Study of the role of chemical support and structured carrier on the CO<sub>2</sub> methanation reaction, *Chem. Eng. J.* 377 (2019) 120461. <https://doi.org/10.1016/j.cej.2018.11.159>.
- [33] P. H. Ho, W. de Nolf, F. Ospitali, A. Gondolini, G. Fornasari, E. Scavetta, D. Tonelli, A. Vaccari, P. Benito, Coprecipitated-like hydrotalcite-derived coatings on open-cell metallic foams by electrodeposition: Rh nanoparticles on oxide layers stable under harsh reaction conditions. *Appl. Catal. A Gen.* 560 (2018) 12–20. <https://doi.org/10.1016/j.apcata.2018.04.014>.
- [34] P. H. Ho, W. de Nolf, F. Ospitali, D. Beton, L. Torkuhl, G. Fornasari, A. Vaccari, P. Benito, Insights into coated NiCrAl open-cell foams for the catalytic partial oxidation of CH<sub>4</sub>, *React. Chem. Eng.* 4 (2019) 1768–1778. <https://doi.org/10.1039/C9RE00178F>.
- [35] H. Muroyama, Y. Tsuda, T. Asakoshi, H. Masitah, T. Okanishi, T. Matsui, K. Eguchi, Carbon dioxide methanation over Ni catalysts supported on various metal oxides, *J. Catal.* 343 (2016) 178–184, <https://doi.org/10.1016/j.jcat.2016.07.018>.
- [36] P. H. Ho, M. Monti, E. Scavetta, D. Tonelli, E. Bernardi, L. Nobili, G. Fornasari, A. Vaccari, P. Benito, Reactions involved in the electrodeposition of hydrotalcite-type compounds on FeCrAlloy foams and plates. *Electrochim. Acta* 222 (2016) 1335–1344. <https://doi.org/10.1016/j.electacta.2016.11.109>.
- [37] F. Basile, P. Benito, G. Fornasari, V. Rosetti, E. Scavetta, D. Tonelli, A. Vaccari, Electrochemical synthesis of novel structured catalysts for H<sub>2</sub> production, *Appl. Catal. B Environ.* 91 (2009) 563–572. <https://doi.org/10.1016/j.apcatb.2009.06.028>.
- [38] H. G. Kim, T. W. Lee, J. Y. Lee, E. S. Lee, K. O. Oh, C. W. Lee, S. H. Lim, Microstructural characterization of Ni-22Fe-22Cr-6Al metallic foam by transmission electron microscopy, *J. Electron Microsc.* (Tokyo), 61 (2012) 299–304. <https://doi.org/10.1093/jmicro/dfs047>.

- [39] I. Pettiti, D. Gazzoli, P. Benito, G. Fornasari, A. Vaccari, The reducibility of highly stable Ni-containing species in catalysts derived from hydrotalcite-type precursors, *RSC Adv.* 5 (2015) 82282–82291. <https://doi.org/10.1039/C5RA13863A>.
- [40] D. Tichit, F. Medina, B. Coq, R. Dutartre, Activation under oxidizing and reducing atmospheres of Ni-containing layered double hydroxides, *Appl. Catal. A Gen.* 159 (1997) 241–258. [https://doi.org/10.1016/S0926-860X\(97\)00085-9](https://doi.org/10.1016/S0926-860X(97)00085-9).
- [41] P. Benito, W. de Nolf, G. Nuyts, M. Monti, G. Fornasari, F. Basile, K. Janssens, F. Ospitali, E. Scavetta, D. Tonelli, A. Vaccari, Role of coating-metallic support interaction in the properties of electrosynthesized Rh-based structured catalysts, *ACS Catal.* 2014, 4, 3779–3790. <https://doi.org/10.1021/cs501079k>.
- [42] P. Aghaei, C. G. Visconti, G. Groppi, E. Tronconi, Development of a heat transport model for open-cell metal foams with high cell densities, *Chem. Eng. J.* 321 (2017) 432–446. <https://doi.org/10.1016/j.cej.2017.03.112>.
- [43] J. Guiler, T. Boeltken, F. Timm, I. Mallol, A. Alarcón, T. Andreu, Pushing the limits of SNG process intensification: high GHSV operation at pilot scale, *ACS Sust. Chem. Eng.* 2020, 8, 8409–8418. <https://doi.org/10.1021/acssuschemeng.0c02642>.
- [44] A. Vita, C. Italiano, L. Pino, P. Frontera, M. Ferraro, V. Antonucci, Activity and stability of powder and monolith-coated Ni/GDC catalysts for CO<sub>2</sub> methanation, *Appl. Catal. B: Environ.* 226 (2018) 384–395. <https://doi.org/10.1016/j.apcatb.2017.12.078>.
- [45] A. Vita, C. Italiano, L. Pino, M. Laganà, M. Ferraro, V. Antonucci, High-temperature CO<sub>2</sub> methanation over structured Ni/GDC catalysts: Performance and scale-up for Power-to-Gas application, *Fuel. Proc. Technol.* 202 (2020) 106365. <https://doi.org/10.1016/j.fuproc.2020.106365>.

- [46] C. Janke, M.S. Duyar, M. Hoskins, R. Farrauto, Catalytic and adsorption studies for the hydrogenation of CO<sub>2</sub> to methane, *Appl. Catal. B Environ.* 152-153 (2014) 184–191, <https://doi.org/10.1016/j.apcatb.2014.01.016>.
- [47] C. Italiano, J. Llorca, L. Pino, M. Ferraro, V. Antonucci, A. Vita, 2020. CO and CO<sub>2</sub> methanation over Ni catalysts supported on CeO<sub>2</sub>, Al<sub>2</sub>O<sub>3</sub> and Y<sub>2</sub>O<sub>3</sub> oxides, *Appl. Catal. B Environ.* 264, 118494. <https://doi.org/10.1016/j.apcatb.2019.118494>.
- [48] S. Ewald, O. Hinrichsen, On the interaction of CO<sub>2</sub> with Ni-Al catalysts, *Appl. Catal. A Gen.* 580 (2019) 71–80. <https://doi.org/10.1016/j.apcata.2019.04.005>.
- [49] L.R. Winter, R. Chen, X. Chen, K. Chang, Z. Liu, S.D. Senanayake, A.M. Ebrahim, J.G. Chen, Elucidating the roles of metallic Ni and oxygen vacancies in CO<sub>2</sub> hydrogenation over Ni/CeO<sub>2</sub> using isotope exchange and in situ measurements, *Appl. Catal. B Environ.* 245 (2019) 360–366. <https://doi.org/10.1016/j.apcatb.2018.12.069>.

## Figure Legends

**Fig. 1.** SEM images of structured catalysts after calcination at 600 °C for 6 h: NiAl (a, a1), NiLaAl (b, b1), NiYAl (c, c1), and NiCeAl (d, d1).

**Fig. 2.** H<sub>2</sub>-TPR profiles of bare NiCrAl foam, NiAl and NiXAl calcined samples.

**Fig. 3.** CO<sub>2</sub> conversion (a) and selectivity in CH<sub>4</sub> and CO (b) on NiAl and NiXAl structured catalysts. Total flow rate 240 mL min<sup>-1</sup>, CO<sub>2</sub>/H<sub>2</sub>/N<sub>2</sub> = 1/4/1 v/v, and GHSV = 38,200 h<sup>-1</sup>.

**Fig. 4.** Catalytic performance in CO<sub>2</sub> methanation on NiAl structured catalyst. Reaction conditions: 6 foams of catalyst (containing 30 mg of coating), and CO<sub>2</sub>/H<sub>2</sub>/N<sub>2</sub> = 1/4/1 v/v. Total flow rates 240, 360, and 480 mL min<sup>-1</sup> for GHSV = 19,100; 28,650; and 38,200 h<sup>-1</sup>, respectively.

**Fig. 5.** a) Temperature profiles at the centerline of NiAl catalyst during the activity test and b) temperature increment versus oven temperature during the activity test on NiAl and NiXAl structured catalysts. Reaction condition: 3 foams, CO<sub>2</sub>/H<sub>2</sub>/N<sub>2</sub> = 1/4/1 v/v and GHSV = 38,200 h<sup>-1</sup>

**Fig. 6.** Stability test on NiLaAl, NiYAl and NiCeAl structured catalysts at 325 °C: a) CO<sub>2</sub> conversion and b) CH<sub>4</sub> and CO selectivity. The first 6 h and the period between 30-40 h are the tests at different oven temperature. Total flow rate 240 mL min<sup>-1</sup>, CO<sub>2</sub> /H<sub>2</sub>/N<sub>2</sub> = 1/4/1 v/v (diluted) and 1/4/0 v/v (concentrated), GHSV = 38,200 h<sup>-1</sup>.

**Fig. 7.** Temperature profiles during the stability tests for: a) NiCeAl, b) NiYAl and c) NiLaAl structured catalysts in total flow rate of 240 mL min<sup>-1</sup> of CO<sub>2</sub>/H<sub>2</sub>/N<sub>2</sub> = 1/4/0 v/v at T<sub>oven</sub> = 325 °C and GHSV = 38,200 h<sup>-1</sup>.

**Fig. 8.** Comparison of catalytic performance in CO<sub>2</sub> methanation on NiCeAl pelletized and structured catalysts: a) CO<sub>2</sub> conversion and b) CH<sub>4</sub> and CO selectivity. Total flow rate 240 mL min<sup>-1</sup>, CO<sub>2</sub>/H<sub>2</sub>/N<sub>2</sub> = 1/4/1 v/v, and GHSV = 38,200 h<sup>-1</sup>. Pellets: 21 mg or 30 mg of NiCeAl catalyst diluted by 470 mg quartz. The space velocity values referred to the amount of catalyst are 680 and 480 L g<sup>-1</sup> h<sup>-1</sup> for 21 and 30 mg of NiCeAl respectively. Foams: 3 foams containing 21 mg of NiCeAl coating. The space velocity value referred to this amount of the coating is 680 L g<sup>-1</sup> h<sup>-1</sup>.

**Fig. 9.** Comparison of temperature profiles of NiCeAl pelletized and structured catalysts in CO<sub>2</sub> methanation. Total flow rate 240 mL min<sup>-1</sup>, CO<sub>2</sub>/ H<sub>2</sub>/N<sub>2</sub> = 1/4/1 v/v, and GHSV = 38,200 h<sup>-1</sup>. Pellets: 21 mg of NiCeAl catalyst diluted by 470 mg quartz. Foams: 3 foams containing 21 mg of NiCeAl coating.

**Fig. 10.** HR-TEM images of spent structured catalysts: NiAl (a, a1), NiLaAl (b, b1), NiYAl (c, c1), and NiCeAl (d, d1). The right column shows HAADF images and the insets present the Ni particle size distributions.

## **Support information**

### **Open-cell foams coated by Ni/X/Al hydrotalcite derived catalysts (X = Ce, La, Y) for CO<sub>2</sub> methanation**

Phuoc Hoang Ho<sup>§</sup>, Giancosimo Sanghez de Luna, Francesca Ospitali, Giuseppe Fornasari, Angelo Vaccari, Patricia Benito\*

Dipartimento Chimica Industriale “Toso Montanari”, Università di Bologna, Viale Risorgimento 4, 40136, Bologna, Italy

<sup>§</sup>Present address: Chemical Engineering, Competence Center for Catalysis, Chalmers University of Technology, S-412 96, Gothenburg, Sweden.

\* [patricia.benito3@unibo.it](mailto:patricia.benito3@unibo.it)

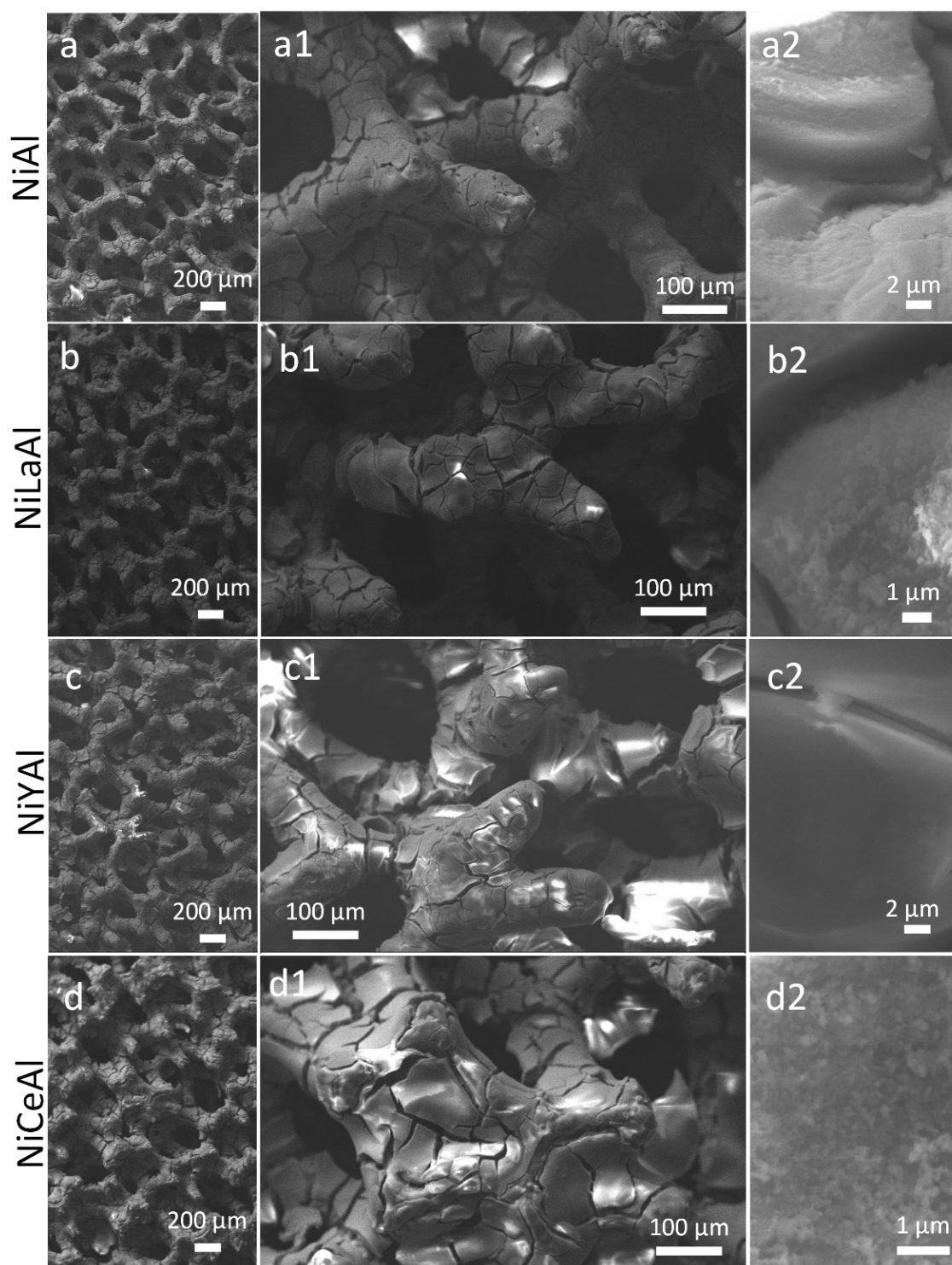


**Fig. S1.** SEM images of foams after electrodeposition at -1.3 V vs SCE for 750 s: NiAl (a, a1, a2), NiLaAl (b, b1, b2), NiYAl (c, c1, c2), and NiCeAl (d, d1, d2).

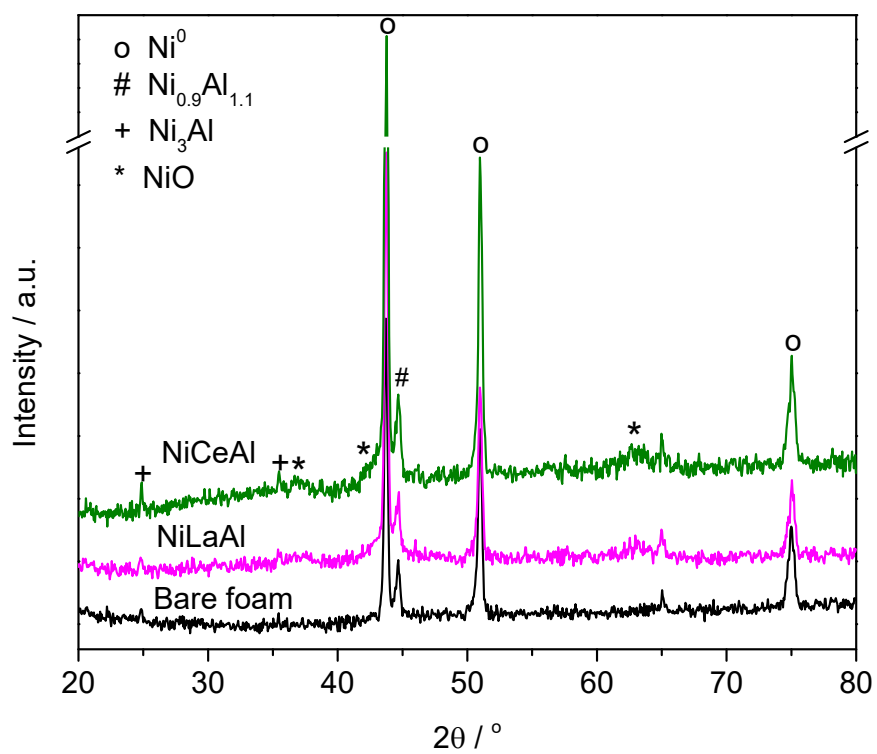


**Fig. S2.** XRD patterns of bare foam, NiLaAl and NiCeAl calcined samples.

The poor crystallinity of the NiO is evidenced by the broad and low intense reflections in the diffraction patterns

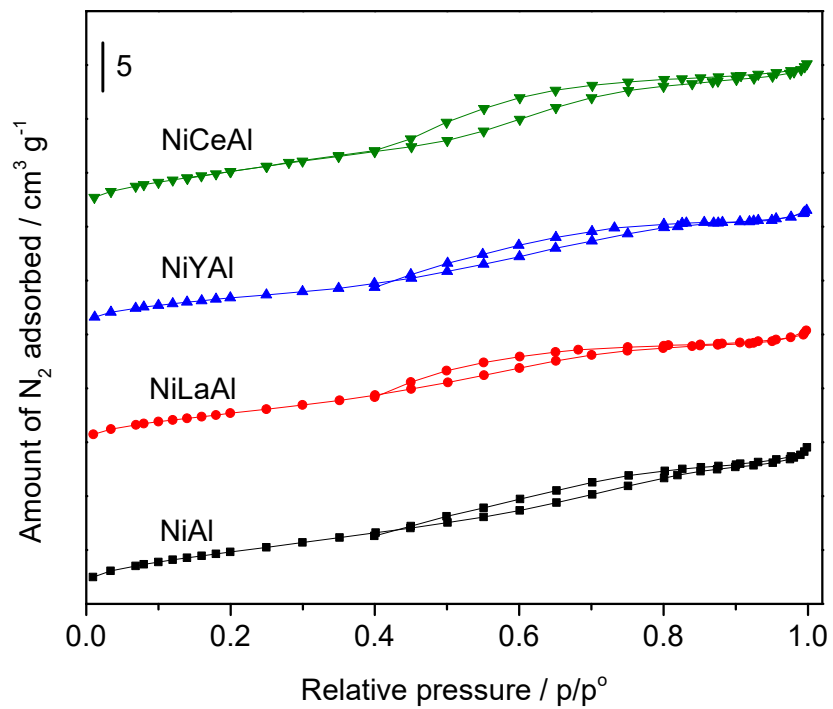


**Fig. S3.**  $N_2$  isotherm adsorption-desorption profiles of NiAl and NiXAl calcined samples.



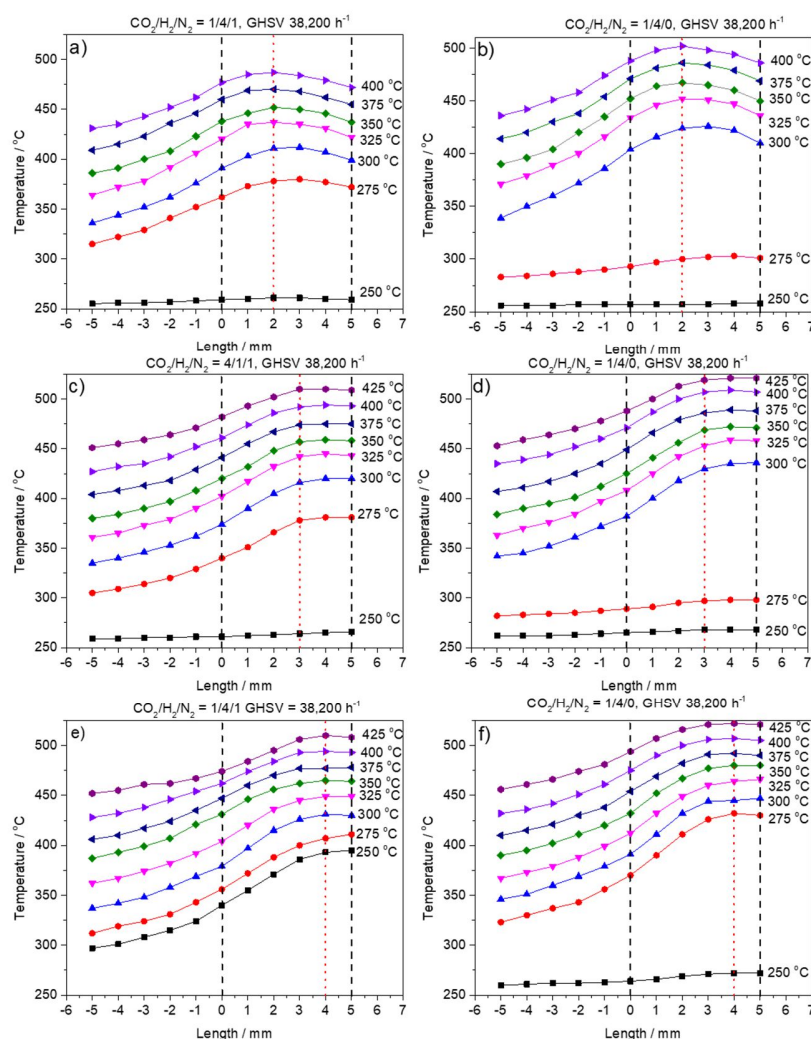


**Fig. S4.** Temperature profiles of NiXAl catalysts recorded along the centerline of the bed during tests feeding diluted ( $\text{CO}_2/\text{H}_2/\text{N}_2 = 1/4/1$  v/v) and concentrated ( $\text{CO}_2/\text{H}_2/\text{N}_2 = 1/4/0$  v/v) gas mixtures: NiLaAl (a, b); NiYAl (c, d); NiCeAl (e, f). Total flow rate  $240 \text{ ml min}^{-1}$  and GHSV =  $38,200 \text{ h}^{-1}$ .

At low oven temperature (250-275 °C), all the catalysts are less active in the concentrated than in diluted feedstock (see Table below), explaining the lower temperatures reached within the catalytic bed under those reaction conditions. Note that heat dispersion upstream the bed slightly increases the measured temperature.

Temperature / °C	Gas mixture $\text{CO}_2/\text{H}_2/\text{N}_2$ v/v	$\text{CO}_2$ conversion %			$\text{CH}_4$ Selectivity %		
		NiLaAl	NiYAl	NiCeAl	NiLaAl	NiYAl	NiCeAl
250	1/4/1	6	6	40	96	98	98
	1/4/0	4	5	5	93	96	96
275	1/4/1	58	61	76	97	97	99
	1/4/0	15	12	12	95	96	96

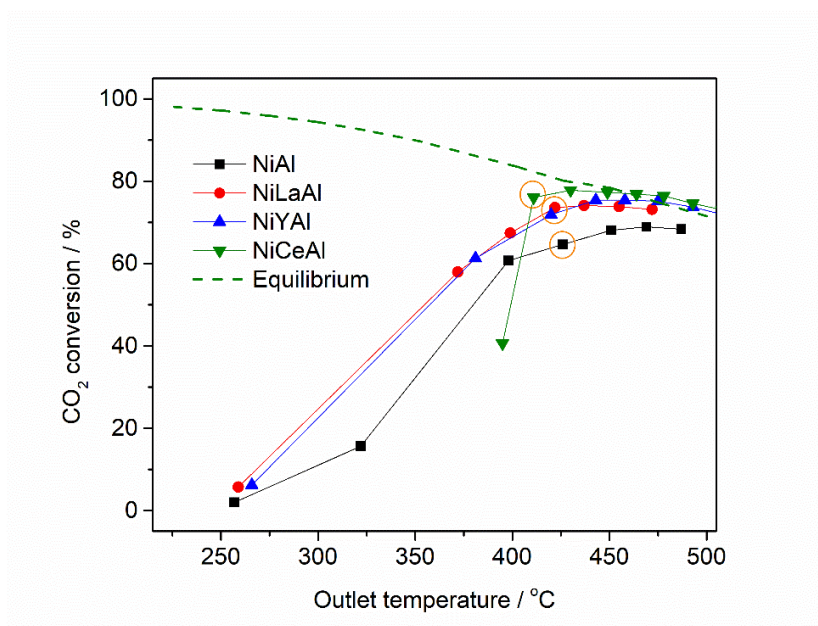


**Fig. S5.** CO<sub>2</sub> conversion versus outlet temperature on different structured catalysts. Total flow rate 240 mL min<sup>-1</sup>, GHSV = 38,200 h<sup>-1</sup>, and CO<sub>2</sub>/H<sub>2</sub>/N<sub>2</sub> = 1/4/1 v/v. Orange circles mark the points corresponding to the oven temperature at 325 °C of each catalyst, suggesting that the conversions at the oven temperature of 325 °C are still far from the thermodynamic equilibrium.

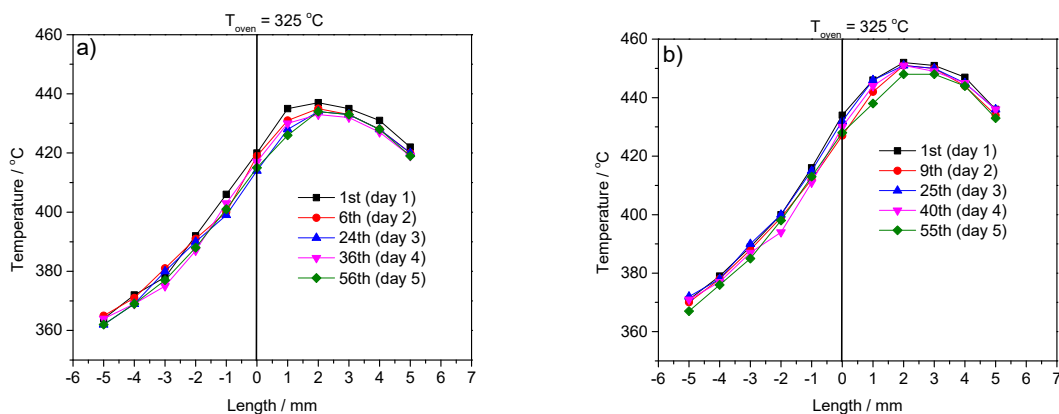


**Fig. S6.** Temperature profiles recorded along the centerline of the bed during tests feeding diluted (a) and concentrated (b) gas mixture during the stability test of NiLaAl catalyst at  $T_{\text{oven}} = 325$  °C. Total flow rate 240 mL min<sup>-1</sup>, GHSV = 38,200 h<sup>-1</sup>, and CO<sub>2</sub>/H<sub>2</sub>/N<sub>2</sub> = 1/4/1 and 1/4/0 v/v for the diluted and concentrated gas mixture, respectively.

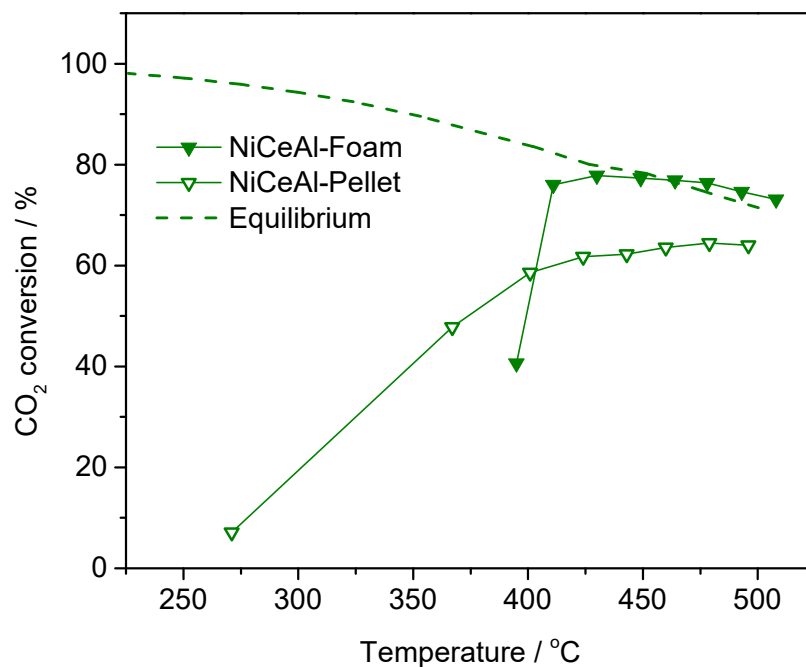


**Fig. S7.** CO<sub>2</sub> conversion versus outlet temperature on NiCeAl pelletized and structured catalyst. Total flow rate 240 mL min<sup>-1</sup>, CO<sub>2</sub>/H<sub>2</sub>/N<sub>2</sub> = 1/4/1 v/v, and GHSV = 38,200 h<sup>-1</sup>. Pellets: 21 mg of NiCeAl catalyst diluted by 470 mg quartz. Foams: 3 foams containing 21 mg of NiCeAl coating.

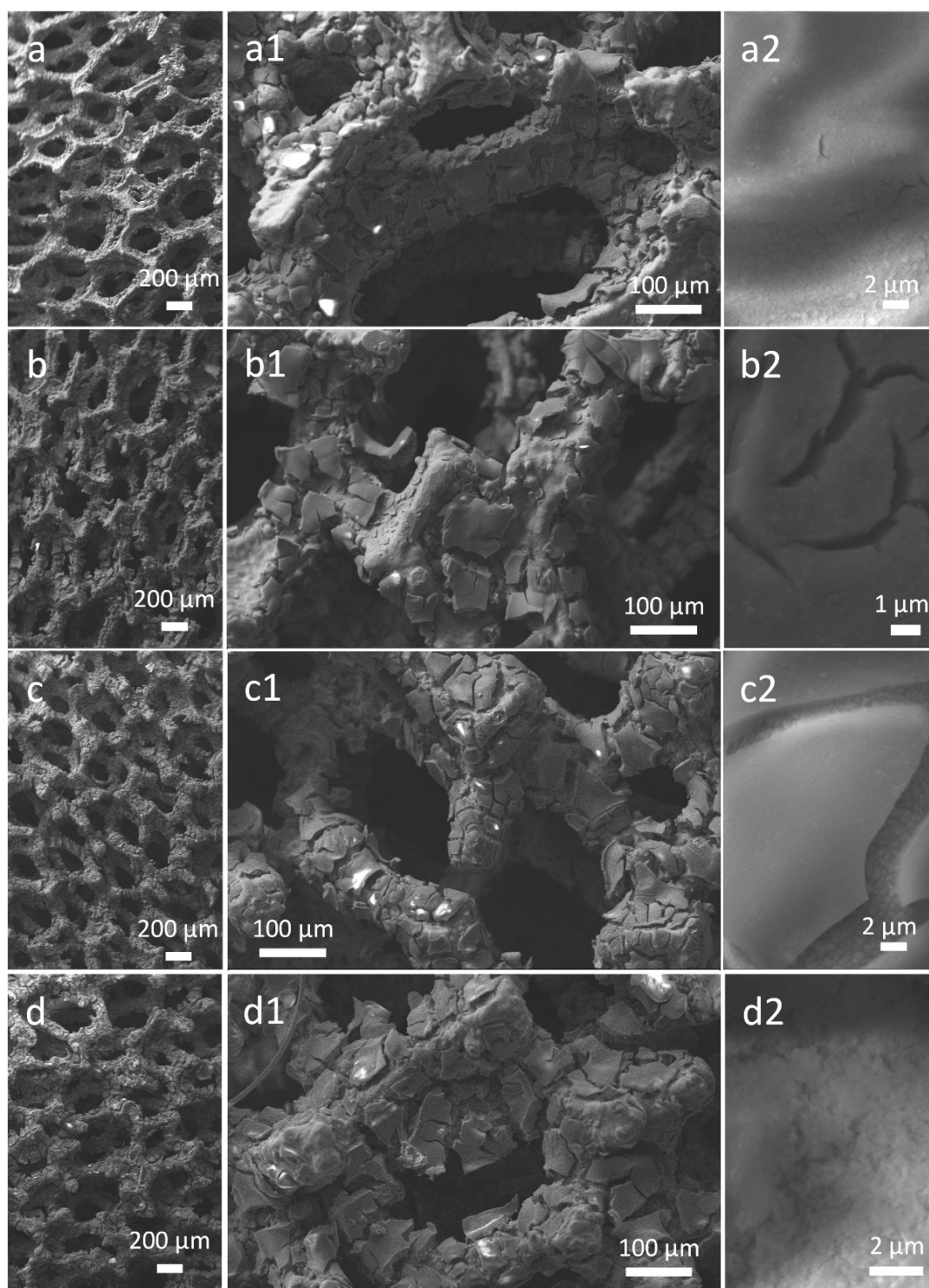


**Fig. S8.** SEM images of structured catalysts after CO<sub>2</sub> methanation tests: NiAl (a, a1, a2), NiLaAl (b, b1, b2), NiYAl (c, c1, c2), and NiCeAl (d, d1, d2).

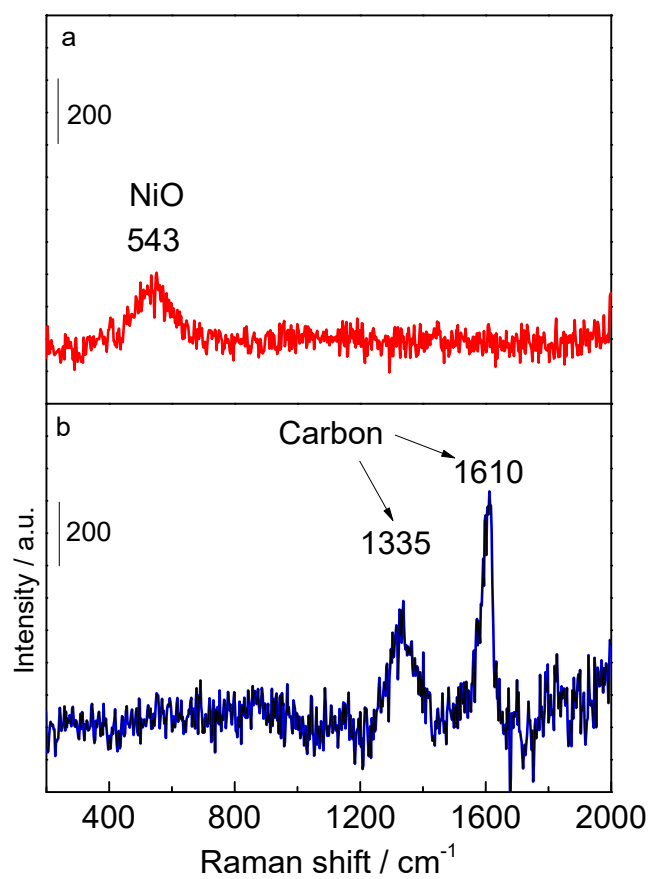


**Fig. S9.** Raman analysis of spent NiAl structured catalyst: a) location without carbon deposition and b) location with carbon formation.

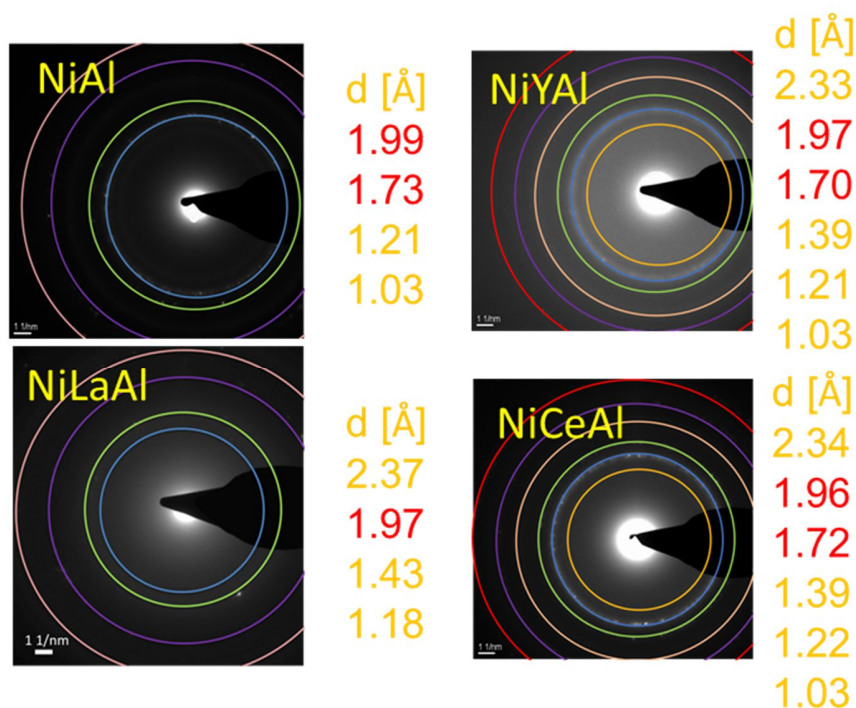
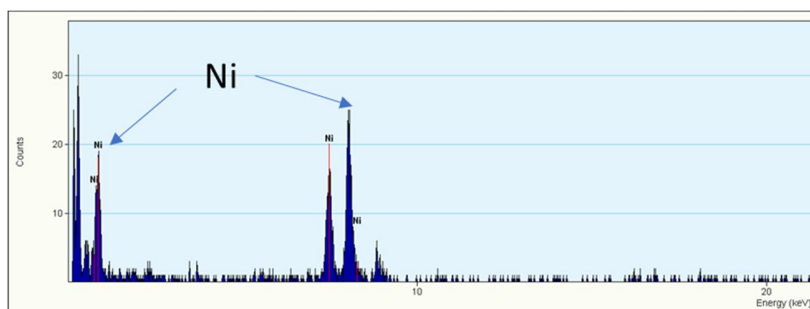
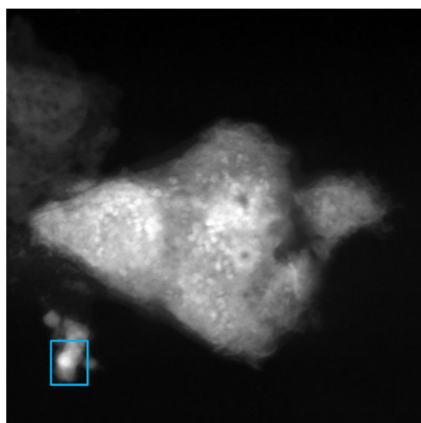


**Fig. S10.** SAED patterns of the spent catalysts.

The NiAl catalyst SAED pattern is related  $\text{Ni}^0$ . The d-spacings at 1.99, 1.73 and 1.22 Å are related to the planes (111), (002), and (022), respectively. [PDF 01-088-2326]. The presence of Ni is also confirmed by STEM/EDS:



The NiLaAl catalyst SAED pattern is related to NiO. The d-spacings at 2.37, 1.97, 1.43, 1.18 have been assigned to the planes (111), (002), (022) and (222). The small domain size of NiO may be responsible of the shift of the d-spacings in comparison to pristine NiO [PDF 01-073-1519]. Since the d spacings for  $\gamma\text{-Al}_2\text{O}_3$  [PDF 01-074-4629] are close to those of NiO, the presence of NiO has been also confirmed by STEM/EDS analysis below:



Element	Weight %	Uncert. %	Atomic %
O (K)	14.97	1.41	39.16
Al (K)	2.02	0.42	3.14
Ni (K)	79.38	2.41	56.59
La (L)	3.60	1.05	1.08

The SAED patterns of NiYAl and NiCeAl catalysts are related to both Ni<sup>0</sup> and NiO, based on the explanations given above for the NiAl and NiLaAl SAED patterns.